This article has been accepted for publication in a future issue of this journal, but has not been fully edited. Content may change prior to final publication. Citation information: DOI 10.1109/TWC.2022.3159086, IEEE Transactions on Wireless Communications

A Holistic Assessment of Directional Deafness in mmWave-based Distributed 3D Networks

Olga Chukhno, Nadezhda Chukhno, Olga Galinina, Sergey Andreev, Yuliya Gaidamaka, Konstantin Samouylov, and Giuseppe Araniti

***Abstract*—The adoption of abundant millimeter-wave (mmWave) spectrum offers higher capacity for short-range connectivity in various Unmanned Aerial Vehicle (UAV)-centric communications scenarios. In contrast to the conventional cellular paradigm, where the coordination of connected nodes is highly centralized, the distributed deployments, such as those operating over unlicensed frequency bands, maintain robust interactions in the absence of central control. These agile decentralized systems are being naturally created by dynamic UAV swarms that form a temporary 3D structure without reliance on remote management or pre-established network infrastructures. While much effort has been invested in the performance assessment of distributed, directional, and 3D systems individually, a combination of these three angles allows capturing more realistic UAV swarm scenarios and produces a novel research perspective. This work addresses one of the fundamental challenges in mmWave-based 3D networks – directional deafness – which is known to adversely affect the overall system performance. Particularly, we develop a mathematical framework by taking into account the peculiarities of 3D directional and distributed deployments. We provide a holistic analytical assessment of directional deafness and propose several powerful approximations that capture realistic antenna patterns.**

***Index Terms*—3D, deafness, directional antenna, distributed networks, stochastic geometry, millimeter wave.**

I. Introduction and Background

A. Research Motivation

The fifth-generation (5G) and beyond communication technology facilitates an expanding range of applications, such as enhanced virtual and augmented reality, industrial control systems, self-driving vehicles, and, notably, autonomous robots and drones. These require increasingly intelligent and effective operations [1] as they impose unprecedented performance demands and may thus encounter radio connectivity challenges. To this end, the next-generation wireless systems adopt communications over extremely high frequency (EHF) bands, such as millimeter-wave (mmWave) spectrum [2] that offers high capacity for short-range connectivity.

In the mmWave spectrum, the use of *highly directional* transmissions is essential to support high antenna gains and, thus, compensate for severe signal attenuation, large atmospheric absorption, and high vulnerability to channel fluctuations [3]. Three-dimensional (3D) beamforming (BF) techniques allow devices to concentrate the transmit power over narrower beams and maintain precise alignment [4] increasing the antenna gain and improving the radio connectivity. In 3D networks that naturally emerge in various Unmanned Aerial Vehicle (UAV)-centric communication scenarios [5], this procedure is of crucial importance due to higher altitudes and faster mobility of the involved drones.

Not limited to mmWave cellular connectivity, the 802.11 Wireless LAN Working Group has recently ratified advanced system specifications [6] that enable high data rate transmissions by expanding the legacy IEEE 802.11ad capabilities [7]. Different from the conventional cellular paradigm, where the coordination of connected nodes is highly centralized, distributed deployments, such as those operating over unlicensed frequency bands, maintain robust interactions in the absence of central control, ownership, or regulation. Here, the centralized connectivity arbitration procedures typically driven by a cellular base station become *distributed* [8], [9]. These decentralized systems are being naturally created by UAV swarms that form a temporary structure without reliance on remote management or pre-established network infrastructures [10].

As UAV swarms are becoming increasingly large and dynamic and require stringent performance guarantees for critical (e.g., merge and split) operations, it becomes essential to enable bandwidth-hungry distributed applications (e.g., in-swarm communications and control convergence). With 2D antenna arrays required by *3D BF techniques*, the number of on-board antenna elements may be increased without exceeding the inherent form-factor limitations, which offers reduced half-power beamwidth (HPBW) and higher antenna gains. The 3D BF allows adapting the beam pattern in both elevation and azimuth planes to exploit more degrees of freedom. Hence, analysis of directional 3D systems is demanded to capture more realistic UAV situations that become commonplace for communications across both UAV-to-UAV and UAV-to-ground links [11]. While much effort has been invested in the performance assessment of distributed, directional, and

O. Chukhno, N. Chukhno, and G. Araniti are with University Mediterranea of Reggio Calabria, Italy and CNIT, Italy. Email: olga.chukhno@unirc.it, nadezda.chukhno@unirc.it, araniti@unirc.it. O. Chukhno, O. Galinina, and S. Andreev are with Tampere University, Finland. Email: olga.galinina@tuni.fi, sergey.andreev@tuni.fi. N. Chukhno is also with Universitat Jaume I, Spain. Yu. Gaidamaka and K. Samouylov are with Peoples' Friendship University of Russia (RUDN University), Russia. Email: gaydamaka-yuv@rudn.ru, samuylov-ke@rudn.ru.

The authors gratefully acknowledge funding from European Union's Horizon 2020 Research and Innovation programme under the Marie Skłodowska Curie grant agreement No. 813278 (A-WEAR: A network for dynamic wearable applications with privacy constraints).

This work was also supported by the Academy of Finland (Projects RADIANT and IDEA-MILL) and by the JAES Foundation (Project STREAM).

This paper has been supported by the RUDN University Strategic Academic Leadership Program (recipient K.S., Section I). The reported study was funded by RSF, project number 22-29-00694 (recipient Yu.G., Section VII).

This work is licensed under a Creative Commons Attribution 4.0 License. For more information, see https://creativecommons.org/licenses/by/4.0/

This article has been accepted for publication in a future issue of this journal, but has not been fully edited. Content may change prior to final publication. Citation information: DOI 10.1109/TWC.2022.3159086, IEEE Transactions on Wireless Communications

3D systems individually, a combination of these three angles produces a novel perspective for the research community. The need for *directional distributed 3D networking* in UAV swarm communications serves as the motivation behind this work.

B. Essential Related Work

Over the recent years, the research community focused efforts on equipping flying platforms with radio communications capabilities by advancing the UAV setups in both centralized [12] and distributed systems [13]. There is already a large body of literature on mmWave-based UAV cellular networking, which includes channel [14] and antenna [15] modeling, coverage analysis [16], 3D beam management [17], positioning [18], trajectory design [19], interference assessment [20], performance optimization [21], experimental studies [22], and UAV prototype development [23].

Despite the benefits of cellular-connected UAV applications, larger UAV swarms require reliable support beyond the coverage of cellular deployments by employing hybrid 3D connectivity. In this context, distributed mmWave-based (e.g., IEEE 802.11ay) solutions have become of growing interest. They can help coordinate drones within a large and dynamic group as it travels through space and changes its configuration. However, the utilization of directional beams in distributed mmWave-based systems introduces unique peculiarities that stem from the notion of directivity [24]. A cornerstone phenomenon is *directional deafness* that occurs where a transmitter fails to communicate to its intended receiver because the latter is beamformed in a different direction [25]. Deafness is typically caused by a lack of state information from the neighboring nodes and may significantly degrade the system performance.

The research work on the coordination of nodes suffering from deafness has accelerated recently but remained focused on directional terrestrial networks. In [26], a channel access protocol that copes with deafness over a single channel and one radio interface was designed. An alternative multi-band approach to address the deafness effects was proposed in [27]. In [28], the use of adequate association together with relaying techniques was shown to alleviate the impact of deafness. In [29], another protocol was coined that combines directional antennas with predictive positioning to overcome deafness. Most recently, the work in [30] aimed to resolve deafness-induced problems by resorting to preamble-based detection mechanisms.

However, a quantitative analysis of directional deafness effects has only been conducted in [31] and, more recently, in [32]. In [31], a deafness probability assessment was proposed for the nodes that are randomly located on a plane. In [32], the authors extended that work to a 3D deployment scenario while controlling the radiation pattern in one plane. A limitation of the existing knowledge is not only in reliance on 2D geometry that applies solely to legacy 2D BF techniques. Past literature also fails to cover the impact of deafness in UAV scenarios, which is increasingly timely as drone formations grow larger, become more distributed, and employ directional antennas. This work aims to bridge the indicated gap by contributing a new mathematical methodology, which brings together distributed UAV communications, directional mmWave connectivity, and 3D BF features with the aim to conduct a holistic deafness probability evaluation.

C. Main Contributions

In this work, by relying upon stochastic geometry tools, we formulate a new methodology for characterizing directional in-swarm UAV communications in the unlicensed bands under realistic assumptions. We deliver a multifaceted analytical assessment of directional deafness in distributed 3D UAV networks. The essential contributions of this study are summarized in more detail as follows.

- We propose an **analytically tractable model** for the antenna pattern represented by a linear function of beamwidth, which mimics realistic radiation patterns and makes it possible to produce closed-form performance estimates. In particular, in this work, we obtain a lower bound for distance-dependent **3D deafness probability**.
- We offer an approximation for the **coverage area** of a **symmetric antenna** as an ellipse, which helps reduce the analysis complexity and improve the accuracy of the results. We assess the tightness of our approximation and establish the parameters required to accurately model the system at hand.
- By further relaxing the assumption on symmetric antenna properties, we develop a more precise yet more complex ellipsoidal approximation of the **coverage area** for antennas with **asymmetric radiation** pattern. By employing this approximation, we offer an expression for the deafness probability in directional UAV systems with arbitrary antenna arrays.
- We extend the methodology for deafness probability evaluation to the case of **arbitrary** real-world deployments of **UAV swarms** and provide selected numerical results to demonstrate its modeling capabilities, thus completing the proposed framework. The provided illustrative example mimics **distributed UAV-to-UAV communications** over the emerging mmWave radio technology by incorporating directionality, decentralized operation, and 3D structure.

The remainder of this text is organized as follows. In Section II, we outline the system modeling assumptions that underpin our subsequent analysis. This is followed by an analytically tractable solution for the deafness probability estimation developed in Section III, which is based on a linear approximation of antennas. Further, our geometry-based approach to the coverage area approximation for both symmetric and asymmetric antennas is detailed in Sections IV and V, respectively. The practical application of the framework is briefly summarized in Section VI. Our numerical evaluation is reported in Section VII. The work concludes in Section VIII.

II. System Model

This section outlines a representative UAV scenario that captures highly directional communications in a distributed 3D setting. We summarize our modeling assumptions on the deployment, antenna radiation pattern, and signal propagation and define the target metrics of interest.

This work is licensed under a Creative Commons Attribution 4.0 License. For more information, see https://creativecommons.org/licenses/by/4.0/

This article has been accepted for publication in a future issue of this journal, but has not been fully edited. Content may change prior to final publication. Citation information: DOI 10.1109/TWC.2022.3159086, IEEE Transactions on Wireless Communications

A. 3D Deployment

We consider a distributed network comprising aerial (e.g., autonomous UAV) and ground (e.g., access point, AP) nodes equipped with highly directional antennas. Particularly, we focus on an open-air scenario where the drones are elevated at different heights within a certain *3D area of interest* as shown in Fig. 1.

For the sake of mathematical tractability, we divide the UAV swarm into more understandable primitives. In this work, a triangle represents the primary building block based on which more complex setups can be analyzed, as discussed in Section VI. Our target example is demonstrated in Fig. 2, where transmitter A (termed *responder*), which may operate as an AP, has established a connection with device B (*primary initiator*). We consider *secondary initiator* C that attempts to connect to the AP (device A) and may experience *directional deafness*.

Assumption 1. *We assume that the location of receiver B is distributed uniformly inside a sphere of radius R_d around A, as shown in Fig. 2a.* Therefore, the probability density function (pdf) and the cumulative distribution function (CDF) of distance r between the connected devices A and B are given by

$$f_r(r) = \frac{3r^2}{R_d^3} \text{ and } F_r(r) = \frac{r^3}{R_d^3}. \tag{1}$$

Spatial locations of target devices A, B, and C form a triangle $\triangle ABC$. We further analyze the deafness problem by considering the plane passing through these three points, as shown in Fig. 2b. For clarity, we denote the angles $\angle BAC$ and $\angle ABC$ as α and β, correspondingly, whereas d is the distance between A and C, d_{BC} is the distance between B and C. Here, α and r are independent random variables, d_{BC} and β depend on r, d, and α as follows from the triangle:

$$d_{BC} = \sqrt{r^2 + d^2 - 2rd\cos\alpha} \text{ and } \beta = \arccos\frac{r - d\cos\alpha}{d_{BC}}. \tag{2}$$

In general, the pdf $f_\alpha(\alpha)$ of angles α converges to the following expression [33]:

$$f_\alpha(\alpha) = \frac{\sin^{n-2}\alpha}{\sqrt{\pi}} \frac{\Gamma\left(\frac{n}{2}\right)}{\Gamma\left(\frac{n-1}{2}\right)}, \alpha \in [0, \pi], \tag{3}$$

where n is the number of space dimensions. For instance, for $n = 2$, $f_\alpha(\alpha) = 1/\pi$, while in our 3D setup, the pdf $f_\alpha(\alpha)$ and the CDF $F_\alpha(\alpha)$ are given as

$$f_\alpha(\alpha) = \frac{\sin\alpha}{2} \text{ and } F_\alpha(\alpha) = \frac{1 - \cos\alpha}{2}, \alpha \in [0, \pi]. \tag{4}$$

Note that the distributions of r, d, and α can vary and rely on the shape of the considered area and the location of A as well as on the spatial distributions of B and C.

B. Realistic Antenna Pattern

Devices A and B are equipped with highly directional transceivers. We assume that a narrow radio beam between A and B is perfectly aligned as a result of employed beamforming procedures, for example, based on compressive sensing [34]. To explicitly model the antenna radiation patterns,

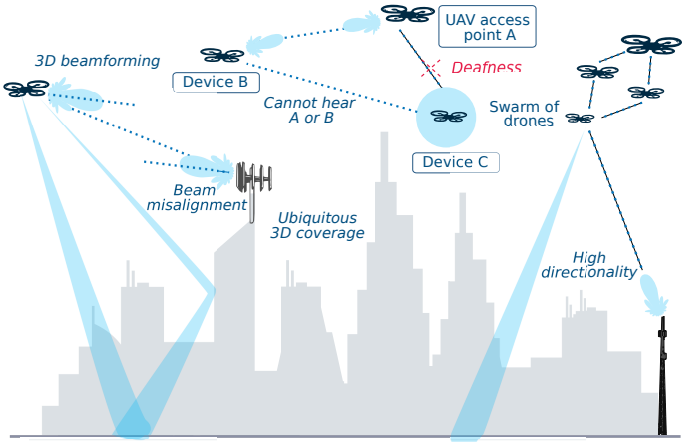

Fig. 1: Illustration of target scenario.

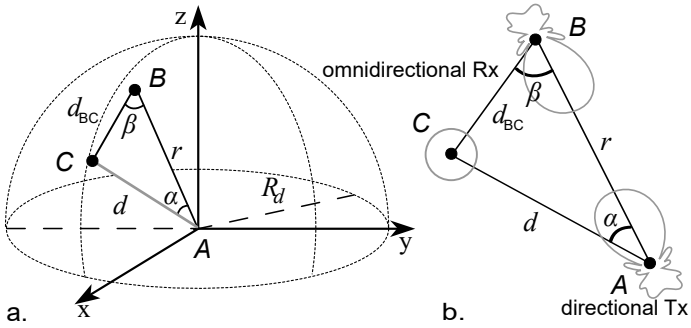

Fig. 2: System model: (a) 3D; (b) planar.

we make the following assumption on symmetric antenna properties.

Assumption 2. *To preserve analytical tractability, we assume that the main antenna lobe is symmetric w.r.t. the antenna boresight axis, i.e., has a symmetric beam pattern in two planes.*

Assumption 2 allows incorporating the randomness of antenna rotation around the boresight axis. The antenna directivity gain D comprises the maximum directivity D_0 along the boresight and a directivity function $\rho(\alpha)$ of the angular deviation from the boresight direction, $\alpha \in [0, \pi]$. Then, the total directivity is defined by $D(\alpha) = D_0\rho(\alpha)$, where $\rho(0) = 1$ corresponds to the antenna boresight.

There are several ways to evaluate the coefficient $\rho(\alpha)$ numerically, namely, by using (i) radiation pattern measurements, (ii) simulation via CEM tools, or (iii) calculation of electromagnetic field produced by specific antenna arrays. It can also be approximated by popular theoretical models, e.g., (i) sector/two-sector antenna pattern for HPBW θ [31], (ii) multi-cosine [35], and (iii) multi-level flat-top antenna patterns [36], or (iv) as outlined in [32] and below.

Assumption 2.1 (linear function). *The function $\rho(\alpha)$ of the relative angle α can be approximated by a piecewise linear function of misalignment of α:*

$$\rho(\alpha) = \begin{cases} 1 - \frac{\alpha}{\theta}, & \alpha \le \theta, \\ 0, & \text{otherwise.} \end{cases} \tag{5}$$

We emphasize that in the proposed approximation, we

This work is licensed under a Creative Commons Attribution 4.0 License. For more information, see https://creativecommons.org/licenses/by/4.0/

This article has been accepted for publication in a future issue of this journal, but has not been fully edited. Content may change prior to final publication. Citation information: DOI 10.1109/TWC.2022.3159086, IEEE Transactions on Wireless Communications

disregard the presence of minor antenna lobes (e.g., side- or backlobes) contrary to the popular model that consists of a sector and a circle of a short radius. A critical drawback of such models that rely on smaller circles is in their trivial cut-off solution [31], which means that they cannot be exploited for the deafness probability analysis.

Assumption 2.2 (directivity gain for symmetric radiation patterns). *Here, we employ an approximation for the radiation pattern in the form of a conical area.* For the HPBW of θ, we may obtain the maximum value of the antenna directivity gain D_0 as a ratio between the solid angle Ω covered by the beam, $\Omega = 2\pi(1-\cos\theta/2)$, and the solid angle of a sphere [37]

$$D_0 = \frac{4\pi}{\Omega} = \frac{2}{1-\cos\frac{\theta}{2}}. \tag{6}$$

To model the coverage area, we formulate the following assumptions.

Assumption 2.3 (coverage area approximation). *We assume that the coverage area of a highly directional antenna has the shape of an ellipse E, $E \equiv < x_0, y_0, a, b >$, where x_0, y_0 are the coordinates of the ellipse center in the horizontal and vertical axes and a, b are the lengths of semiaxes.* Then, the standard equation of an ellipse is determined in Cartesian coordinates as

$$\frac{(x-x_0)^2}{a^2} + \frac{(y-y_0)^2}{b^2} = 1. \tag{7}$$

This approximation for the coverage area of a directional antenna by an ellipse is advantageous in terms of (i) reduction in analysis complexity and (ii) increase in simulation accuracy for symmetric antennas subject to adequate selection of ellipse parameters, which is described in Section IV. To further account for more complex antenna patterns, we adopt the following assumptions.

Assumption 3. *For the case of asymmetric antenna configurations with 2D antenna elements (see Fig. 3), sufficient steering capability is provided in both horizontal and vertical planes by taking into account HPBW for the azimuth and elevation angles.*

Assumption 3.1 (directivity gain for asymmetric radiation patterns). *Here, we assume that antenna directivity can be determined as $D_0 \approx \frac{4\pi}{\theta_{az}\theta_{el}}$* [37], where θ_{az} is the HPBW in the horizontal plane and θ_{el} is the HPBW in the vertical plane.

Assumption 3.2 (coverage area approximation). *We assume that the shape of 3D coverage area of a directional antenna is represented by an ellipsoid $E_{3\text{-}axial} \equiv < x_0, y_0, z_0, a, b, c >$ with center (x_0, y_0, z_0) and semiaxis lengths (a, b, c). The ellipsoid is characterized by*

$$\frac{(x-x_0)^2}{a^2} + \frac{(y-y_0)^2}{b^2} + \frac{(z-z_0)^2}{c^2} = 1. \tag{8}$$

We demonstrate the difference between symmetric and asymmetric antenna properties w.r.t. the deafness probability and confirm the feasibility of the above assumptions in Section VII.

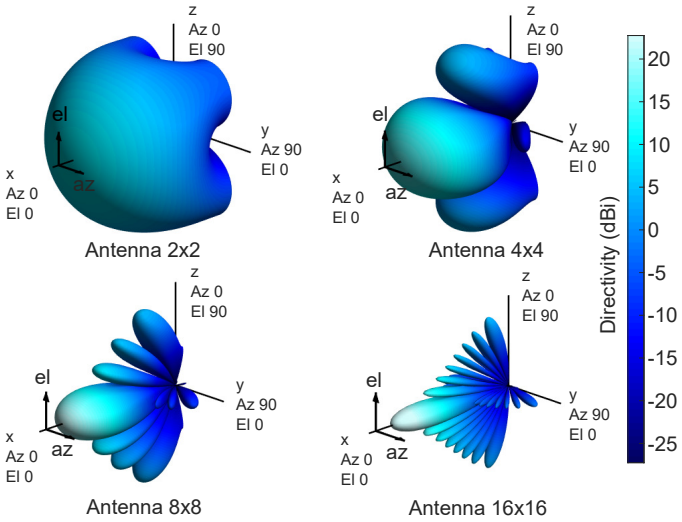

Fig. 3: Visualization of 3D directivity pattern for uniform rectangular arrays with isotropic antenna elements of size 2x2, 4x4, 8x8, and 16x16 with Chebyshev tapering, no steering.

C. Propagation Characterization

We assume that nodes A and B transmit in the directional mode and C listens omnidirectionally, as per IEEE 802.11ad/ay specifications w.r.t. the connection establishment [38]–[40]. Directional reception would require sweeping through all combinations of receiving and transmitting antenna codebooks and result in overheads, which may prohibit efficient UAV support.

Assumption 4. *The average path loss can be calculated as $L(d) = Cd^{\kappa}$, where d is the distance between the transmitter and the receiver, κ is the path loss exponent that depends on the environment, $C = (4\pi/\lambda)^2$ is the propagation constant, and λ is the wavelength.*

The received power can then be calculated as

$$P_{\text{rx}} = P_{\text{tx}} G_{\text{tx}} G_{\text{rx}} L^{-1}(d) = \frac{P_{\text{tx}} D_0 \rho(\alpha)}{Cd^{\kappa}}, \tag{9}$$

where P_{tx} is the transmit power, $G_{\text{tx}} = D_0\rho(\alpha)$ and $G_{\text{rx}} = 1$ are transmit and receive antenna gains. The sensitivity P_{thr} determines the minimum power required by the control physical-layer functions [38]. Therefore, to calculate the radius of the coverage area R, we substitute $d = R$ and $P_{\text{rx}} = P_{\text{thr}}$ into (9) as $R = \left(\frac{P_{\text{tx}} D_0}{P_{\text{thr}} C}\right)^{\frac{1}{\kappa}}$.

D. Directional Deafness

We define directional deafness as a situation where a UAV attempts to communicate with an active device (UAV AP) and fails because it is unable to sense the medium busy during the RTS/CTS handshake procedure employed in IEEE 802.11 systems. In our three-device setup, A and B are connected, beamformed toward each other, and actively exchange data, whereas C aims to establish a connection with A. While attempting to access the medium, device C may face the following outcomes:

This work is licensed under a Creative Commons Attribution 4.0 License. For more information, see https://creativecommons.org/licenses/by/4.0/

This article has been accepted for publication in a future issue of this journal, but has not been fully edited. Content may change prior to final publication. Citation information: DOI 10.1109/TWC.2022.3159086, IEEE Transactions on Wireless Communications

1) Device C receives a signal from either A or B (the received power from A or B exceeds the sensitivity threshold, i.e., $P_{\text{rx,A}} \geq P_{\text{thr}}$ or $P_{\text{rx,B}} \geq P_{\text{thr}}$).
2) Device C fails to receive a signal from A and B, or both received powers $P_{\text{rx,A}}$ and $P_{\text{rx,B}}$ at C are lower than the minimum threshold, i.e., $P_{\text{rx,A}} < P_{\text{thr}}$ and $P_{\text{rx,B}} < P_{\text{thr}}$. In this case, device C may interpret the absence of a response from A as an indication of a collision and retransmit repeatedly, which leads to an inflated backoff time and eventually to a packet drop. We refer to this event as to *directional deafness*.

Hereinafter, we evaluate the deafness probability, i.e., the probability that secondary initiator C fails to communicate with responder A as antenna beams of both A and primary initiator B are directed toward each other:

$$P_D = \Pr\{P_{\text{rx,A}} < P_{\text{thr}}, P_{\text{rx,B}} < P_{\text{thr}}\}. \tag{10}$$

Our system model introduces a set of assumptions to capture the essential directionality effects in 3D distributed UAV networks. The proposed framework goes beyond a particular area-of-interest shape and may capture any 3D configuration (e.g., an ellipsoid, a hemisphere, a dodecahedron, etc.) across random drone swarm layouts. Based on these assumptions, we first obtain a closed-form lower bound on the 3D distance-dependent deafness probability by applying a linear antenna approximation (Section III). This approximation represents a simple-to-use function for the misplacement of the antenna directivity, which is compatible with the existing solutions (sector, etc.). Then, we approximate the coverage area of a symmetric antenna as an ellipse (Section IV). We derive an expression for the more complex asymmetric antenna model that characterizes the coverage area (ellipsoid-based), which is representative of real-world UAV systems (Section V). We elaborate on our methodology for analyzing directional deafness effects by adapting it to practical UAV deployments (Section VI).

III. Deafness Probability Analysis

In this section, we offer a general formulation for the deafness probability, which can be analyzed numerically. We also obtain the respective lower bound represented by a closed-form expression for the antenna patterns approximated according to (5).

A. Distance-Dependent Deafness Probability

First, we derive a general expression for the directional deafness probability in a 3D system.

Proposition 1. *For a fixed distance of d between responder A and secondary initiator C in a space of any dimension and given radius R_d of the area of interest, the deafness probability averaged over spatial locations of initiator B can be expressed by*

$$P_D(d) = \int_0^{\pi}\int_0^{R_d} I\left(\rho(\alpha) < \frac{d^\kappa}{R^\kappa}, \rho(\beta) < \frac{d_{BC}^\kappa}{R^\kappa}\right) f_r(r) f_\alpha(\alpha)\, dr d\alpha, \tag{11}$$

where $I(.)$ is an indicator function and β and d_{BC} are given by (2)*.*

Proof. The proof is based on the received power in the omnidirectional reception mode (9):

$$\begin{aligned} P_D(d) &= \Pr\{P_{\text{rx,A}} < P_{\text{thr}}, P_{\text{rx,B}} < P_{\text{thr}}\} \\ &= \Pr\left\{\frac{P_{\text{tx}} D_0 \rho(\alpha)}{C d^\kappa} < \frac{P_{\text{tx}} D_0}{C R^\kappa}, \frac{P_{\text{tx}} D_0 \rho(\beta)}{C d_{BC}^\kappa} < \frac{P_{\text{tx}} D_0}{C R^\kappa}\right\} \\ &= \Pr\left\{\rho(\alpha) < \frac{d^\kappa}{R^\kappa}, \rho(\beta) < \frac{d_{BC}^\kappa}{R^\kappa}\right\} \\ &= \int_0^{\pi}\int_0^{R_d} I\left(\rho(\alpha) < \frac{d^\kappa}{R^\kappa}, \rho(\beta) < \frac{d_{BC}^\kappa}{R^\kappa}\right) f_r(r) f_\alpha(\alpha)\, dr d\alpha. \end{aligned} \tag{12}$$

□

Corollary 1. *If locations of device B are distributed uniformly within a sphere of radius R_d, and $f_r(r)$, $f_\alpha(\alpha)$ follow (1) and (4), correspondingly, the deafness probability is given by:*

$$P_D(d) = \frac{3}{2R_d^3} \int_0^{\pi}\int_0^{R_d} I\left(\rho(\alpha) < \frac{d^\kappa}{R^\kappa}, \rho(\beta) < \frac{d_{BC}^\kappa}{R^\kappa}\right) r^2 \sin\alpha\, dr d\alpha. \tag{13}$$

Proof. The proof follows from Proposition 1. □

Expression (13) provides an approximation that can be applied to different types of antenna radiation patterns by selecting an appropriate reduction factor $\rho(\alpha)$ that captures the decrease in power due to deviation α from the boresight axis.

B. Lower Bound on Deafness Probability

The use of the linear antenna pattern approximation (5) permits the derivation of a simple and analytically tractable solution in a closed form.

Proposition 2. *If locations of B are distributed uniformly within a sphere of radius R_d and linear function* (5) *approximates the antenna directivity, then a lower bound on the probability of deafness at a fixed distance of d may be obtained as follows:*

For shorter distances $d \leq R_d \sin\theta$,

$$\begin{aligned} P_D(d | d \leq R_d \sin\theta) = \frac{d^3 \cot\theta}{32 R_d^3 \sin^2\theta} \Bigg[& 2\sin\left(\frac{4\theta R^\kappa - 2d^\kappa\theta}{R^\kappa}\right) \\ & - \sin\left(\frac{6\theta R^\kappa - 4d^\kappa\theta}{R^\kappa}\right) + 4\sin\left(\frac{2\theta R^\kappa - d^\kappa 2\theta}{R^\kappa}\right) - 2\sin\left(\frac{2\theta d^\kappa}{R^\kappa}\right) + 6\pi \\ & + \sin\left(\frac{4\theta R^\kappa - d^\kappa 4\theta}{R^\kappa}\right) + \sin\left(\frac{4d^\kappa\theta - 2\theta R^\kappa}{R^\kappa}\right) - 12\theta + \frac{12\theta d^\kappa}{R^\kappa}\Bigg], \end{aligned} \tag{14}$$

or, otherwise, for $d > R_d \sin\theta$,

$$P_D(d | d > R_d \sin\theta) = \frac{\cos\tilde{z}_1 - \cos\tilde{z}_2}{2} + \frac{d^3}{64 R_d^3 \sin^3\theta}\Bigg[12\cos\theta$$

This work is licensed under a Creative Commons Attribution 4.0 License. For more information, see https://creativecommons.org/licenses/by/4.0/

This article has been accepted for publication in a future issue of this journal, but has not been fully edited. Content may change prior to final publication. Citation information: DOI 10.1109/TWC.2022.3159086, IEEE Transactions on Wireless Communications

$$\left[\left(\frac{d^\kappa\theta}{R^\kappa}-\theta+\tilde{z}_1\right)+\left(\frac{d^\kappa\theta}{R^\kappa}-\theta-\tilde{z}_2+\pi\right)\right]+6\sin\left(3\theta-\frac{2d^\kappa\theta}{R^\kappa}\right)$$
$$-6\sin\left(\frac{2d^\kappa\theta}{R^\kappa}-\theta\right)+2\sin\left(5\theta-\frac{2d^\kappa\theta}{R^\kappa}\right)-2\sin\left(\frac{2d^\kappa\theta}{R^\kappa}+\theta\right)$$
$$-\sin\left(7\theta-\frac{4d^\kappa\theta}{R^\kappa}\right)+\sin\left(\frac{4d^\kappa\theta}{R^\kappa}-\theta\right)-6\sin(\theta+2\tilde{z}_1)$$
$$+6\sin(\theta+2\tilde{z}_2)-2\sin(3\theta+2\tilde{z}_1)+2\sin(3\theta+2\tilde{z}_2)$$
$$+\sin(3\theta+4\tilde{z}_1)-\sin(3\theta+4\tilde{z}_2)\Big], \quad (15)$$

where $z_{1,2}=\pm 2\arctan\left(\frac{\sqrt{-\frac{R_d^2}{d^2}\tan^2\theta+\tan^2\theta+1}\pm 1}{(\frac{R_d}{d}+1)\tan\theta}\right)$,
$\tilde{z}_1=\max\{z_1,\theta(1-\frac{d^\kappa}{R^\kappa})\}$, $\tilde{z}_2=\min\{z_2,\pi-\theta(1-\frac{d^\kappa}{R^\kappa})\}$.

Proof. The proof is detailed in [32]. □

IV. Ellipse-based Approach: Symmetric Antennas

In this section, we outline a *geometric* approach to the analysis of directional deafness probability by employing an ellipse as an approximation of the coverage area.

A. General Description

We study a three-node system, which represents a minimal feasible set that can be extended to arbitrary deployments as discussed in Section VI. We consider two ellipses, $E_A(a,0,a,b)$ and $E_B(r-\frac{R}{2},0,a,b)$, which correspond to the coverage areas of devices A and B, and circle $E_C(0,0,d,d)$ that denotes the locus of point C as illustrated in Fig. 4. We further define the deafness zones for device C.

Our approach is to evaluate the deafness probability as a ratio between the weighted arc length of the deafness zone and the length of the semicircle. Below, we define the locus of points in the deafness zone in Lemma 1; the formulation for the deafness probability in our 3D UAV deployment follows in Proposition 3 and Corollary 2.

B. Estimation of Directional Deafness Probability

Lemma 1. *The locus of node locations in the deafness zone is given by the arcs of circle $E_C(0,0,d,d)$ bounded by points A_i, B_i, where the circle intersects two ellipses $E_A(a,0,a,b)$ and $E_B(r-\frac{R}{2},\pi,a,b)$. Here, angle α belongs to the area*

$$\Omega_\alpha=\begin{cases}\gamma_1<\alpha<\pi-\gamma_2, & d^*<d\le R-r,\\ \gamma_1<\alpha<\pi, & R-r<d\le R,\end{cases}$$
$$\Rightarrow \Omega_\alpha=\gamma_1<\alpha<\pi-\gamma_2, \quad (16)$$

where $\gamma_1=\arcsin\frac{\max(y_{A_1},y_{B_1})}{d}$, $\gamma_2=\arcsin\frac{y_{B_2}}{d}$; $A_i(x_{A_i},y_{A_i}), B_i(x_{B_i},y_{B_i})$ are the intersection points of E_C and E_A, E_B and their corresponding coordinates, and d^* is the maximum distance between A and C that allows C to remain inside the ellipse corresponding to B as indicated in Fig. 4.

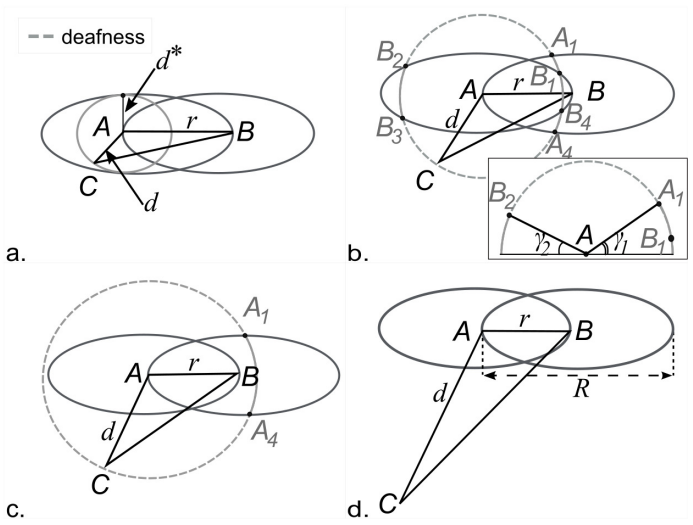

Fig. 4: Possible deafness situations (dashed curves represent deafness zones).

Proof. The coordinates of the intersection points of the ellipses and the circle can be established from the following systems of equations:

$$\begin{cases}\frac{(x-a)^2}{a^2}+\frac{y^2}{b^2}=1,\\ x^2+y^2=d^2,\end{cases} \text{ and } \begin{cases}\frac{\left(x-r+\frac{R}{2}\right)^2}{a^2}+\frac{y^2}{b^2}=1,\\ x^2+y^2=d^2.\end{cases} \quad (17)$$

Solving the former system, we obtain the roots (18)–(20) that correspond to the intersection points A_1, A_2 of the locus circle and the ellipse related to device A. Similarly, we solve the second system for the locus circle and the ellipse related to device B and obtain the coordinates of points B_1, B_2, B_3, B_4 as provided in (21)–(23). The coordinates are as follows:

$$x_{A_{1,2}}=-\frac{1}{2}\frac{Rb^2\mp a\sqrt{S}}{a^2-b^2}, \quad (18)$$

$$y_{A_{1,2}}=\frac{b}{2(a^2-b^2)}\sqrt{P\pm 2Ra\sqrt{S}}, \quad (19)$$

$$y_{A_{3,4}}=-\frac{b}{2(a^2-b^2)}\sqrt{P\mp 2Ra\sqrt{S}}, \quad (20)$$

$$x_{B_{1,2}}=\frac{1}{2}\frac{Rb^2-2b^2r\pm a\sqrt{S-4Rb^2r+4b^2r^2}}{a^2-b^2}, \quad (21)$$

$$y_{B_{1,2}}=\frac{b}{2(a^2-b^2)}\sqrt{P+N\mp 2(Ra-2ar)(S-4Rb^2r+4b^2r^2)^{1/2}}, \quad (22)$$

$$y_{B_{3,4}}=-\frac{b}{2(a^2-b^2)}\sqrt{P+N\pm 2(Ra-2ar)(S-4Rb^2r+4b^2r^2)^{1/2}}, \quad (23)$$

where $S=4b^4+(R^2-4a^2)b^2+4(a^2-b^2)d^2$, $P=-R^2a^2+4a^4-(R^2+4a^2)b^2-4(a^2-b^2)d^2$, and $N=-4(a^2+b^2)r^2+4(Ra^2+Rb^2)r$.

Hence, depending on distance d, we have the following possible options:

- no deafness and no equation roots if $d<d^*$ or no deafness and 2 roots if $d=d^*$ (see Fig. 4a),
- 2 deafness zones and 6 roots if $d^*<d\le R-r$ (see Fig. 4b),
- 1 deafness zone and 2 roots if $R-r<d\le R$ (see Fig. 4c),

This work is licensed under a Creative Commons Attribution 4.0 License. For more information, see https://creativecommons.org/licenses/by/4.0/

This article has been accepted for publication in a future issue of this journal, but has not been fully edited. Content may change prior to final publication. Citation information: DOI 10.1109/TWC.2022.3159086, IEEE Transactions on Wireless Communications

- full deafness and no equation roots if $d > R$ (see Fig. 4d).

Here, d^* represents the maximum distance between A and C that allows C to remain inside the ellipse corresponding to B (no deafness) and is calculated from the zero discriminant of $(b^2-a^2)x^2-2\left(\frac{R}{2}-r\right)b^2x+b^2\left(\frac{R}{2}-r\right)^2+a^2d^2-a^2b^2=0$ as $d^*=\frac{b}{2}\sqrt{\frac{-R^2+4a^2-4b^2+4Rr-4r^2}{a^2-b^2}}$. □

Utilizing the result of Proposition 1, we arrive at the method of calculating the deafness probability under the assumption of symmetric antennas. This means that the main antenna lobe is symmetric w.r.t. the antenna boresight axis and that the antenna pattern in both horizontal and vertical planes remains the same (i.e., has approximately cone shape).

Proposition 3. *For any device C in any space dimension, the deafness probability at a fixed distance of d can be approximated as follows:*

$$P_D(d)=\int\limits_{\alpha\in\Omega_\alpha}\int\limits_{0}^{R_d} f_r(r)f_\alpha(\alpha)\,dr d\alpha, \tag{24}$$

where α represents $\angle BAC$, Ω_α is interpreted as (16), $f_r(r)$ and $f_\alpha(\alpha)$ follow from (1) and (4).

Proof. The proof follows from the definition of the deafness probability and Lemma 1 based on the assumption on the symmetry of our model w.r.t. the horizontal axis:

$$P_D(d)=\int\limits_{0}^{\pi}\int\limits_{0}^{R_d} I(\gamma_1<\alpha<\pi-\gamma_2)f_r(r)f_\alpha(\alpha)\,dr d\alpha. \tag{25}$$

□

Corollary 2. *For devices located in 3D space, the deafness probability may be derived as*

$$P_D(d)=\frac{3}{2R_d^3}\int\limits_{0}^{R_d} r^2\left[\sqrt{1-\frac{\max\left(y_{A_1},\,y_{B_1}\right)^2}{d^2}}+\sqrt{1-\frac{y_{B_2}^2}{d^2}}\right]dr, \tag{26}$$

where y_{A_1} is given by (20), and y_{B_1}, y_{B_2} correspond to (22).

Proof. For the 3D case, we substitute $f_r(r)=3r^2/R_d^3$ (1) and $f_\alpha(\alpha)=\sin(\alpha)/2$ (4) into (24), integrate, and readily obtain

$$\begin{aligned}P_D(d)&=\frac{3}{2R_d^3}\int\limits_{0}^{R_d} r^2\,dr\int\limits_{\gamma_1}^{\pi-\gamma_2}\sin(\alpha)\,d\alpha\\&=\frac{3}{2R_d^3}\int\limits_{0}^{R_d} r^2\left[\cos\gamma_1-\cos(\pi-\gamma_2)\right]dr,\end{aligned} \tag{27}$$

where $\gamma_1=\arcsin\frac{\max(y_{A_1},\,y_{B_1})}{d}$, $\gamma_2=\arcsin\frac{y_{B_2}}{d}$. Further, we obtain the deafness probability from the numerical integration of (27). □

To implement the proposed ellipse-based approach in UAV scenarios of an arbitrary dimension, it is essential to (i) identify the intersection points of geometrical figures that determine the coverage area of A and B, and the locus of locations of C; (ii) based on (20), (22), and (23), calculate angles γ_1 and γ_2 that correspond to the arc lengths of non-deafness zones and find the deafness zones on the semicircle; (iii) define the indicator function $I(\Omega_\alpha)$ by taking into account d and r; and (iv) assign weights to the values of angle α according to (4).

C. Parametrization of Ellipse-based Model

Here, we address the derivation of the parameters for each ellipse in the proposed UAV scenario with three nodes. The major semiaxis a of the ellipse equals half of the maximum distance R between the transmitter and the receiver, at which a radio link can be maintained:

$$a=\frac{1}{2}\left(\frac{P_{\text{tx}}D_0}{P_{\text{thr}}C}\right)^{\frac{1}{\kappa}}=\frac{R}{2}. \tag{28}$$

Then, b may be produced from (7) with $x=\cos(\theta/2)\;d_{\text{hpbw}}$ and $y=\sin(\theta/2)\;d_{\text{hpbw}}$, where d_{hpbw} is the distance between the antenna and the half-power points (-3dB) as detailed in Fig. 5. It can be derived from the following relationship:

$$\frac{G(\theta)}{G_{\max}}=0.5=\frac{d_{\text{hpbw}}^{\kappa}}{R^{\kappa}}\Rightarrow d_{\text{hpbw}}=0.5^{1/\kappa}R, \tag{29}$$

where $G_{\max}$ is the maximum gain and $G(\theta)=G_{\max}/2$.

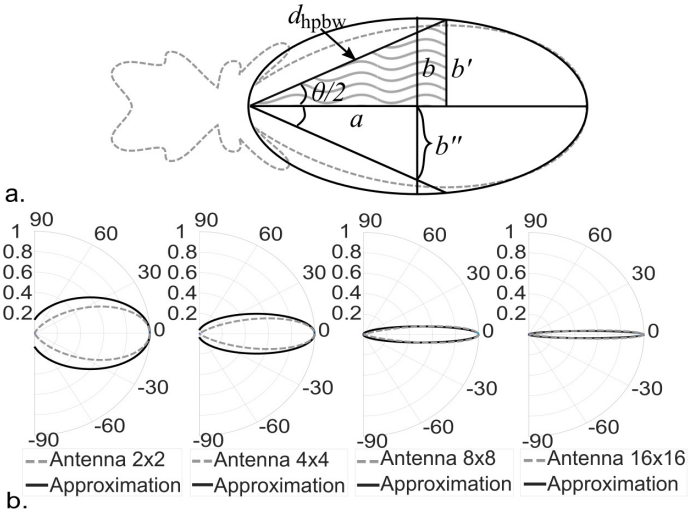

Fig. 5: Ellipse as coverage area approximation: (a) geometrical abstraction; (b) antenna approximation (5) (solid line) for uniform rectangular arrays (dashed) in polar coordinate system.

By substituting the parameters a, x, and y into (7), we characterize the minor semiaxis b as:

$$b=\frac{y}{\sqrt{1-\frac{(x-x_0)^2}{a^2}}}=\frac{\sin(\theta/2)\;R\;0.5^{1/\kappa}}{\sqrt{1-\frac{(\cos(\theta/2)\;R\;0.5^{1/\kappa}-x_0)^2}{(R/2)^2}}}. \tag{30}$$

However, realistic antenna patterns are closer to the form of *a drop* (dotted pattern in Fig. 5) rather than an ellipse (line), and depend on the beamwidth. Hence, we can obtain b' from the upper triangle through hypotenuse d_{hpbw} from (29) and angle $\theta/2$:

$$b'=\sin(\theta/2)\;R\;0.5^{1/\kappa}. \tag{31}$$

We also formulate a more coarse approximation for b, which may be derived from the bottom triangle. Here, by analogy, we have angle $\theta/2$ and the adjacent cathetus a. Then,

$$b''=\tan(\theta/2)\;a. \tag{32}$$

This work is licensed under a Creative Commons Attribution 4.0 License. For more information, see https://creativecommons.org/licenses/by/4.0/

This article has been accepted for publication in a future issue of this journal, but has not been fully edited. Content may change prior to final publication. Citation information: DOI 10.1109/TWC.2022.3159086, IEEE Transactions on Wireless Communications

In practice, an antenna pattern might have no definite form; therefore, we validate and analyze our results against realistic settings in Appendix.

V. Ellipsoid-based Approach: Asymmetric Antennas

In this section, we derive formulations for more practical but complex antenna models, i.e., those that are not symmetric w.r.t. the antenna boresight (referred to as asymmetric antennas). We characterize the shape of the coverage area for devices A and B as an ellipsoid (see Fig. 6).

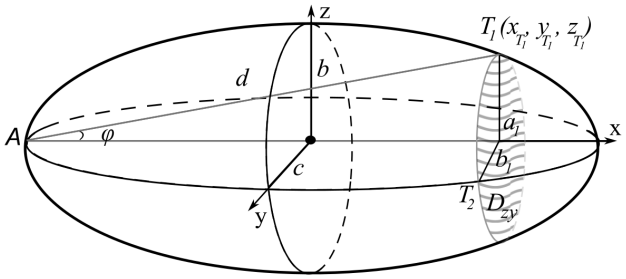

Fig. 6: Ellipsoid as approximation of coverage area for asymmetric antennas.

A. General Description and Parametrization

We consider the intersection of an ellipsoid that approximates the coverage area of a device (A or B) and a sphere that reflects the possible locations of device C:

$$\begin{cases} \frac{(x-x_0)^2}{a^2} + \frac{y^2}{b^2} + \frac{z^2}{c^2} = 1, \\ x^2 + y^2 + z^2 = d^2, \end{cases} \tag{33}$$

where semiaxis a corresponds to (28) from the ellipse-based approach, b corresponds to (30), (31), or (32) with $\theta = \theta_{\text{az}}$, and semiaxis c can be obtained from (30), (31), or (32) by substituting θ_{el} into θ. In other words, the ellipsoid projections are two ellipses in azimuth and elevation planes with semiaxes a, b and a, c, correspondingly.

We define the deafness probability via the surface area, which is not cut by ellipsoids (A and B) from the sphere. Importantly, we derive the general expressions for both ellipsoids A and B with the centers along the X-axis at x_0. Note that the ellipsoid that approximates the coverage area of device A is centered at $(a, 0, 0)$. In the case of device B, the center of the ellipsoid is $(r - R/2, 0, 0)$ by analogy with the ellipse-based approach.

B. Deafness Probability Estimation

We estimate the deafness probability by assessing the outer area of the solid of intersection of the sphere and the ellipsoids. We determine the surface area of the spherical cap inside the ellipsoid as a non-deafness zone, while the outer pieces of the sphere represent deafness zones.

Proposition 4. *Depending on distance d, the deafness probability can be obtained from*

$$P_D(d) = \int_0^{R_d} \left(1 - \frac{S_{\text{B,left}}(\sigma) + \max\left(S_{\text{A,right}}(\sigma), S_{\text{B,right}}(\sigma)\right)}{4\pi d^2}\right) f_r(r)\, dr, \tag{34}$$

where $S_{\text{A,right}}(\sigma), S_{\text{B,right}}(\sigma), S_{\text{B,left}}(\sigma)$ are the sought surfaces of the sphere bounded by ellipsoids A and B (from the right and the left sides), respectively; $f_r(r)$ follows (1).

Proof. Let surface σ be defined by the expression $x{=}f(z, y)$ and its projection onto the plane zOy is the region D_{zy}. Then, the area of the surface σ is determined by

$$S(\sigma) = \iint_{D_{zy}} \sqrt{1 + \left(\frac{\partial x}{\partial z}\right)^2 + \left(\frac{\partial x}{\partial y}\right)^2}\, dz\, dy. \tag{35}$$

The proof of this proposition is structured as follows. First, we determine the plane projection D_{zy} of surface σ. Then, we proceed with the surface σ and define the surface area of the portion of the sphere inside the ellipsoid.

Projection: Plane projection D_{zy} of surface σ is an ellipse with semiaxes a_1 and b_1 (see Fig. 6). To obtain the intersection curve (ellipse) that defines D_{zy}, we consider each of the horizontal E_{h} and vertical E_{v} ellipses of the ellipsoid separately for the sake of exposition. Therefore, for the vertical plane, we characterize the intersection of ellipse E_{v} with the equation of a line:

$$\begin{cases} \frac{(x-x_0)^2}{a^2} + \frac{z^2}{c^2} = 1, \\ z = x \tan\phi_{\text{el}}. \end{cases} \tag{36}$$

To establish the intersection point $T_1(x_{T_1}(x_0), 0, z_{T_1}(x_0))$ of line d with ellipse E_{v}, we solve (36):

$$x_{T_1}(x_0) = \frac{c^2 x_0 \pm \sqrt{a^2 c^2 (c^2 + a^2 \tan^2\phi_{\text{el}} - x_0^2 \tan^2\phi_{\text{el}})}}{c^2 + a^2 \tan^2\phi_{\text{el}}},$$
$$z_{T_1}(x_0) = \tan\phi_{\text{el}}\, x_{T_1}(x_0). \tag{37}$$

In the case of device A, coordinates of T_1 can be transformed into $\left(\frac{2ac^2}{c^2 + a^2\tan^2\phi_{\text{el}}}, 0, \frac{2ac^2\tan\phi_{\text{el}}}{c^2 + a^2\tan^2\phi_{\text{el}}}\right)$. Since $x_{T_1}^2 + z_{T_1}^2 = d^2$, we obtain $\phi_{\text{el}}(x_0)$ as follows:

$$\phi_{\text{el}}(x_0) = \pm\arctan\sqrt{\frac{c^2(-a^2d^2x_0^2 + c^2U_1) - 2ac^2d^2x_0U_2}{a^4U_3 - 2a^2c^2x_0^2(c^2 - d^2) + c^4x_0^4}}, \tag{38}$$

$$\phi_{\text{el}}(x_0) = \pm\arctan\sqrt{\frac{c^2(-a^2d^2x_0^2 + c^2U_1) + 2ac^2d^2x_0U_2}{a^4U_3 - 2a^2c^2x_0^2(c^2 - d^2) + c^4x_0^4}}, \tag{39}$$

where $U_1 = (-a^4 + x_0^2(2a^2 + d^2 - x_0^2) + a^2d^2) + d^2(a^4 - a^2d^2)$, $U_2 = \sqrt{(c^2 - a^2)(c - d)(c + d) + c^2x_0^2}$, $U_3 = (c^4 - 2c^2d^2 + d^4)$.

Similarly, we solve the system of equations for ellipse E_{h} and equation of a straight line:

$$\begin{cases} \frac{(x-x_0)^2}{a^2} + \frac{y^2}{b^2} = 1, \\ y = x \tan\phi_{\text{az}}. \end{cases} \tag{40}$$

For brevity, we omit the derivation details and expressions for $x_{T_2}(x_0)$, $y_{T_2}(x_0)$, $\phi_{\text{az}}(x_0)$.

This work is licensed under a Creative Commons Attribution 4.0 License. For more information, see https://creativecommons.org/licenses/by/4.0/

This article has been accepted for publication in a future issue of this journal, but has not been fully edited. Content may change prior to final publication. Citation information: DOI 10.1109/TWC.2022.3159086, IEEE Transactions on Wireless Communications

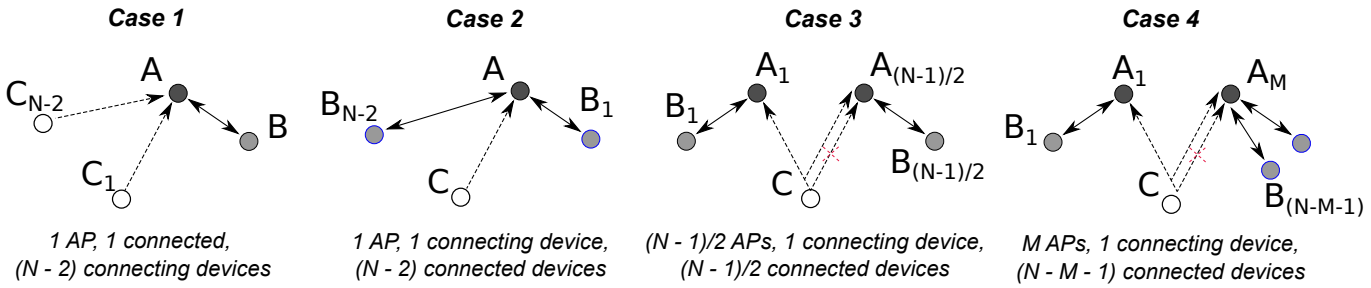

Fig. 7: Illustration of N-node setup.

The projection D_{zy} of surface σ onto plane zOy is an ellipse with semiaxes $a_1(x_0)$=$z_{T_1}(x_0)$ and $b_1(x_0)$=$y_{T_2}(x_0)$:

$$\frac{z^2}{a_1(x_0)^2}+\frac{y^2}{b_1(x_0)^2}=1, \tag{41}$$

where $a_1(x_0)=\tan\phi_{\text{el}}\, x_{T_1}(x_0)$ and $b_1(x_0)=\tan\phi_{\text{az}}\, x_{T_2}(x_0)$.

Surface σ: Further, we formulate the expression for σ, which bounds the ellipsoid. Since $x=\sqrt{d^2-y^2-z^2}$, the partial derivatives of x with respect to z and y can be obtained from

$$\frac{\partial x}{\partial z}=-\frac{z}{\sqrt{d^2-y^2-z^2}} \text{ and } \frac{\partial x}{\partial y}=-\frac{y}{\sqrt{d^2-y^2-z^2}}. \tag{42}$$

The surface integral over projection σ onto plane zOy has the following form

$$S(\sigma)=\iint\limits_{D_{zy}}\frac{d}{\sqrt{d^2-y^2-z^2}}\,dz\,dy. \tag{43}$$

To calculate (43), we transition to the polar coordinate system by replacing the variables $z=\rho\cos\phi$, $y=\rho\sin\phi$, $\rho^2=z^2+y^2$, and $dzdy=\rho d\rho d\phi$. Hence, (43) transforms to

$$S(\sigma)=\iint\limits_{D_{\rho\phi}}\frac{d}{\sqrt{d^2-\rho^2}}\rho\,d\rho\,d\phi. \tag{44}$$

As ellipse equation determines the limits of integration, the outer ones are 0 and 2π, while the inner integration limits can be derived from

$$\frac{(\rho\cos\phi)^2}{a_1(x_0)^2}+\frac{(\rho\sin\phi)^2}{b_1(x_0)^2}=1$$

$$\Rightarrow \rho=\pm\frac{a_1(x_0)b_1(x_0)}{\sqrt{a_1(x_0)^2\sin^2\phi+b_1(x_0)^2\cos^2\phi}}. \tag{45}$$

Consequently, the surface of the sphere bounded by the ellipsoid can be established from

$$S(\sigma)=\int\limits_0^{2\pi}d\phi\int\limits_0^{\frac{a_1(x_0)b_1(x_0)}{\sqrt{a_1(x_0)^2\sin^2\phi+b_1(x_0)^2\cos^2\phi}}}\frac{d}{\sqrt{d^2-\rho^2}}\rho\,d\rho\,. \tag{46}$$

Then, the sought surface is given by the following expression:

$$S(\sigma)=\frac{2(\pi a_1(x_0)^2d^2-\pi b_1(x_0)^2d^2-\pi d|a_1(x_0)^2d-b_1(x_0)^2d|)}{a_1(x_0)^2-b_1(x_0)^2}. \tag{47}$$

Importantly, we characterize the surface area cut by the ellipsoid given by $(x-x_0)^2/a^2+y^2/b^2+z^2/c^2=1$ from the sphere $x^2+y^2+z^2=d^2$. We obtain surface region (47) bounded by the intersection curves, which represents the non-deafness zone. Note that ellipsoid A cuts one (or two) part(s) out of the sphere depending on distance r, while ellipsoid B and sphere C have only one intersection curve. Therefore, the deafness probability can be obtained via the numerical integral (34). □

VI. Practical Considerations

In this section, we summarize the extensions of our methodology for practical use. Given the reference three-device setup, we consider the following cases that cover all possibilities to construct an N-node UAV system as illustrated in Fig. 7.

1) Case 1: The N-node system comprises $(N-2)$ devices of type C, one device A, and one device B. In this case, the deafness probability $P_D(d)$ depends only on distance d. The resulting expression is the same for any device $C_i, i=1,...,N-2$, i.e., corresponds to (10), which is averaged over all possible locations of B. Due to averaging, we further refer to the cases where there is only one device of type C in the system.

2) Case 2: The N-node system comprises one device A, which communicates with $(N-2)$ devices of type B, while one device C aims to connect to A. Here, there are two options:

Case 2.1: Success of C depends on $B_i, i=1,...,N$, which is active when C activates. Since the deafness probability is averaged over all possible locations of B_i and, thus, does not depend on i, the resulting expression for this subcase corresponds to (10). This operation mode is foreseen to be the most utilized in 802.11ad/ay networks.

Case 2.2: Device A is equipped with multiple beams to communicate with $(N-2)$ devices of type B and serves them simultaneously. This subcase implies multi-user multiple-input multiple-output (MU-MIMO) operation, which is uncommon but can be supported by, e.g., the emerging IEEE 802.11ay protocol [40]. The deafness probability, i.e., the probability that secondary initiator C fails to communicate with responder A as antenna beams of device A direct toward $B_i, i=1,...,N$ is given by

$$P_D=\Pr\{P_{\text{rx},A}^{(1)}<P_{\text{thr}}, P_{\text{rx},B_1}<P_{\text{thr}},...,$$

$$P_{\text{rx},A}^{(N-2)}<P_{\text{thr}}, P_{\text{rx},B_{N-2}}<P_{\text{thr}}\},$$

This work is licensed under a Creative Commons Attribution 4.0 License. For more information, see https://creativecommons.org/licenses/by/4.0/

This article has been accepted for publication in a future issue of this journal, but has not been fully edited. Content may change prior to final publication. Citation information: DOI 10.1109/TWC.2022.3159086, IEEE Transactions on Wireless Communications

where $P^{(i)}_{\text{rx},A}$ represents the received power (at C) from A when it transmits to B_i, P_{rx,B_i} is the received power from B_i, and the maximum power budget of A is split among $(N-2)$ devices of type B.

3) Case 3: The N-node system comprises $\frac{N-1}{2}$ devices of type A, $\frac{N-1}{2}$ devices of type B (each A is connected to one B), and one device C that aims to join the system. Device C attempts to connect to one of devices A_i at a time. The target AP A_i is selected according to a certain association rule, which defines the shape of the distribution of distances d between C and A_i. If the same association rule is adopted across the entire network, i.e., employed also by primary initiators B_i, then it as well affects spatial locations of B_i around A_i and should be carefully taken into account.

Case 3.1: No coordination in the system of beams between A_i and B_i. The success of C depends on the pair A_i and B_i. We, thus, have

$$P_D = \Pr\{P_{\text{rx},A_1} < P_{\text{thr}}, P_{\text{rx},B_1} < P_{\text{thr}}, ..., P_{\text{rx},A_{\frac{N-1}{2}}} < P_{\text{thr}}, P_{\text{rx},B_{\frac{N-1}{2}}} < P_{\text{thr}}\}. \quad (48)$$

The deafness probability in the case of random deployments of devices of type A is of particular interest from the network point of view and is analyzed numerically in Section VII. We note that it is also possible to find analytical solutions for particular types of deployments of A_i given the distribution of distances from C to $A_i, i = 1, ..., \frac{N-1}{2}$. The simplest case of Poisson Point Process (PPP) of A_i locations yields independent distances d and results in factorization of (48), while deployments with more deterministic structure, such as grid, might require introducing further approximations.

Case 3.2: There is coordination between APs A_i. For example, the IEEE 802.11ad/ay amendment supports clustering of distributed APs to mitigate high interference between them [41]. Such clustering allows a group of APs to schedule their transmissions in non-overlapping time periods, thereby allowing co-channel APs to coordinate beaconing and avoid interference in dense environments. This subcase is more complex as it includes spatial correlation between the active beams and, particularly, locations of active B_i. However, it could be approximated via thinning of the point process of A_i locations.

Case 4: Finally, we consider a union of all the above cases as an N-mode system comprising M devices of type A, $N-M-1$ devices of type B, and one device C. Then, the deafness probability corresponds to the union of cases. For example, for cases 2.2 and 3.1, it can be formulated as

$$P_D = \Pr\{P^{(1)}_{\text{rx},A_1} < P_{\text{thr}}, P_{\text{rx},B_1} < P_{\text{thr}}, ..., P^{(N-M-1)}_{\text{rx},A_M} < P_{\text{thr}}, P_{\text{rx},B_{N-M-1}} < P_{\text{thr}}\},$$

where $P^{(j)}_{\text{rx},A_i}$ represents the received power (at C) from A_i when it transmits to B_j, P_{rx,B_i} is the received power from B_i. Presented cases cover the entire event space for directional deafness evaluation in a realistic UAV environment. We note that at a particular instant, device C may also receive high interference from AP A_j, other than the target A_i. In this case, we assume that C senses the channel as occupied and does not attempt to initiate a transmission. Such event is not classified as network-based deafness as there is no deafness w.r.t. A_j; however, in this case, the deafness probability would be lower than the deafness estimated in a three-node system.

VII. Numerical Analysis

This section collects important numerical results on analyzing the deafness probability in 3D directional and distributed UAV systems. We illustrate the capabilities of our proposed framework under assumptions of symmetric and asymmetric radiation patterns. Furthermore, we study the impact of antenna pattern rotation and system parameters on the deafness probability. The validation of our framework by comparing the results of the proposed mathematical approximations against those obtained via simulations for realistic antenna radiation patterns is detailed in Appendix.

A. Simulation Setup and System Parameters

As an illustrative example, we consider a UAV swarm elevated at different altitudes within the *area of interest* of radius R_d (see Fig. 1, Fig. 2). Other nodes are served by a UAV AP equipped with, e.g., novel IEEE 802.11ay chipsets, which provide reliable high-rate connectivity in a noise-limited environment [42]. Following the recommendations from the available standardization documents [6], [38], [39], we assume the fixed transmit power of $P_{\text{tx}} = 23\,\text{dBm}$, while the receive power exceeds the threshold $P_{\text{thr}} = -78\,\text{dBm}$ that corresponds to the lowest modulation and coding scheme (MCS0).

To accurately capture the performance of real-world UAV deployments, we employ the path loss model with $\kappa = 2.25$ as the propagation of 60 GHz signals exhibits higher losses for aerial links [9]. We assume uniform rectangular and linear arrays (URAs/ULAs) of isotropic/cosine elements; the antenna patterns are constructed using MATLAB Sensor Array Analyzer. The remaining system parameters are summarized in Table I.

B. Practical Setup Analysis

We begin by evaluating the proposed analytical framework for the N-node scenario and the antenna patterns that are symmetric w.r.t. the boresight axis. To this aim, we employ 2x2, 4x4, 8x8, 16x16, 32x32, and 64x64 URAs of isotropic antenna elements. We analyze the probability of deafness for cases 3.1, 2.2, and 4 outlined in Section VI as demonstrated in Fig. 8, Fig. 9, and Fig. 10, respectively.

TABLE I: Summary of main parameters

Notation	Description	Value
f	Carrier frequency	60 GHz
λ	Wavelength	0.005 m
κ	Propagation exponent	2.25 [9]
C	Propagation constant	$6.3165 \cdot 10^6$
P_{thr}	Sensitivity	-78 dBm [39]
P_{tx}	Transmit power	23 dBm
θ	Beamwidth	var
R_d	Area of interest radius	var

This work is licensed under a Creative Commons Attribution 4.0 License. For more information, see https://creativecommons.org/licenses/by/4.0/

This article has been accepted for publication in a future issue of this journal, but has not been fully edited. Content may change prior to final publication. Citation information: DOI 10.1109/TWC.2022.3159086, IEEE Transactions on Wireless Communications

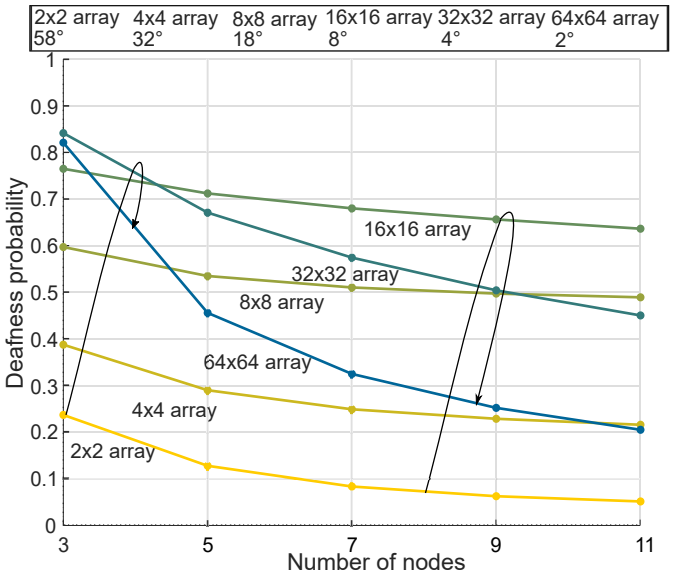

Fig. 8: Deafness probability vs. distance d between A and C: N-node system comprising $(N-1)/2$ devices A, $(N-1)/2$ devices B, and one device C (Case 3.2).

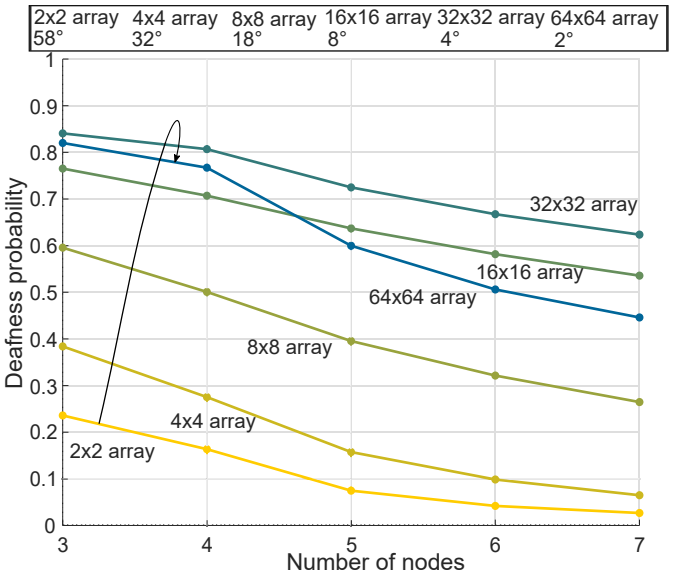

Fig. 9: Deafness probability vs. distance d between A and C: N-node system comprising one device A, $(N-2)$ devices B, and one device C (Case 2.2).

First, we employ multi-connectivity degrees ranging from 1 to 5 while assuming the use of IEEE 802.11ad/ay decentralized clustering. We compare the deafness probability for the case of $N = 3, 5, 7, 9, 11$, i.e., 1 to 5 devices of type A, 1 to 5 devices of type B, and one device C that aims to establish a connection. In this scenario, devices A are distributed according to a PPP. In Fig. 8, the deafness probability is illustrated as a function of the number of nodes N. We observe that the increase in N leads to reduced deafness probability for this particular case with distributed coordination mechanisms. We then analyze the case with a highly directional multi-beam antenna design on the AP side. In Fig. 9, we demonstrate the probability of deafness for the case of $N = 3, 4, 5, 6, 7$, i.e., one device A, 1 to 5 devices of type B, and one device C. As one may observe, multi-user operation compensates deafness probability offering more options to avoid communication failures for device C.

To complement the discussion, we demonstrate the deafness probability for case 4 in Fig. 10. As a general trend, one may notice that the system performance depends on the antenna array size. For instance, 32x32 and 64x64 URAs are more vulnerable to deployment density in terms of deafness probability and demonstrate up to 95% deafness probability reduction with an increase in the number of devices. In practice, the operator may consider the choice of the beam resolution that might be related to a particular deployment and the required level of reliability. We emphasize that densification in the systems with coordination among APs should not degrade the system performance due to the interference. In contrast, densification without coordination may increase the number of collisions leading to system operation failures.

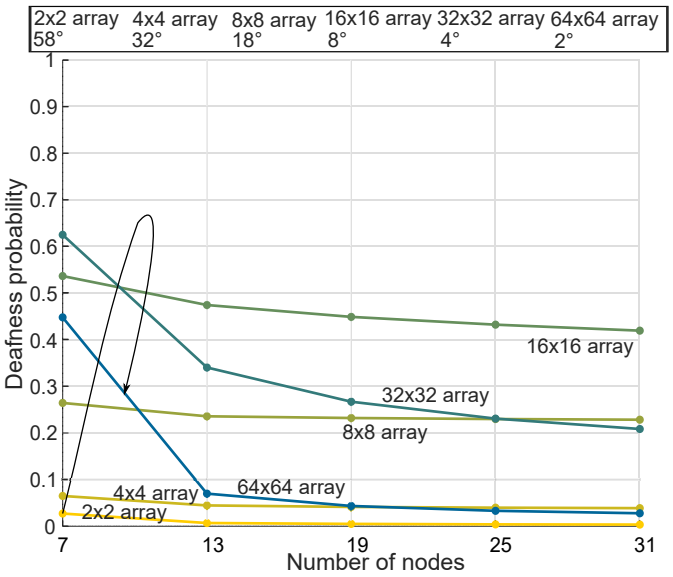

Fig. 10: Deafness probability vs. distance d between A and C: N-node system comprising M devices of type A, $(N-M-1)$ devices B, and one device C (Case 4).

C. Effects of Antenna Pattern Rotation

One of the benefits of our ellipsoid-based approach is that it captures the properties of asymmetric antennas. In Fig. 11, we illustrate the deafness probability for ULA. We observe that the curves display behavior similar to that of URAs. Particularly, the deafness probability declines down to 50% for the ULA consisting of 4 isotropic antenna elements. We emphasize that the methods with centrally symmetric approximations of antenna patterns might not apply to linear arrays. In contrast, the ellipsoid-based approximation as per (34) allows modeling a wider range of antennas and, hence, facilitates the analysis of various mmWave-based UAV systems.

This work is licensed under a Creative Commons Attribution 4.0 License. For more information, see https://creativecommons.org/licenses/by/4.0/

This article has been accepted for publication in a future issue of this journal, but has not been fully edited. Content may change prior to final publication. Citation information: DOI 10.1109/TWC.2022.3159086, IEEE Transactions on Wireless Communications

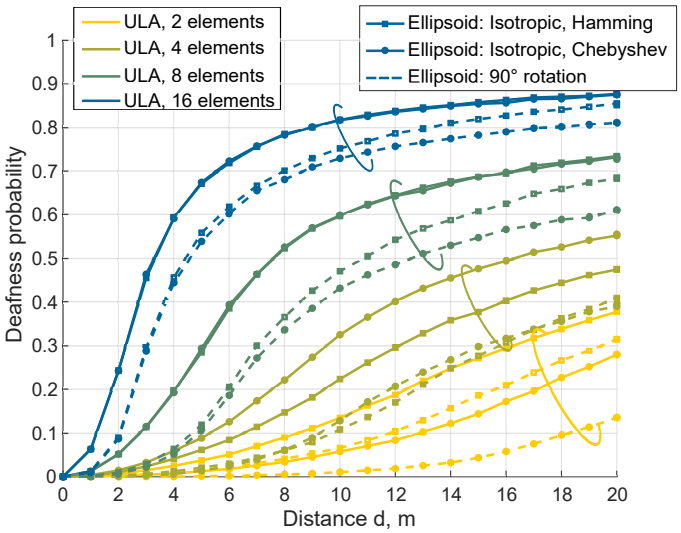

Fig. 11: Impact of variations in antenna settings and antenna pattern rotation.

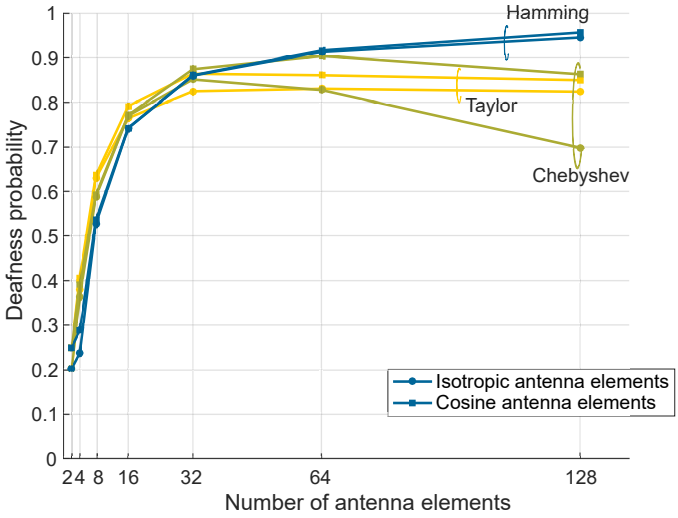

Fig. 12: Impact of antenna array size.

We study the impact of beam rotation on the deafness probability, as illustrated in Fig. 11. We employ different antenna patterns of linear arrays for the ellipsoid-based coverage area approximation and rotate ellipsoid B through 90° about the X-axis. As one may observe, such antenna rotation reduces the deafness probability in the case of asymmetric antennas. For symmetric URA antennas, the deafness probability exhibits a consistent behavior irrespectively of the UAV axial movement. This suggests a conclusion that representation of many real-life scenarios requires modeling 2D antenna array in 3D and confirms that the proposed framework can effectively capture in-swarm UAV communications. We note that an imperfect alignment of antenna beams of the transmitter and the primary initiator (A and B) may have effects on the deafness probability; however, this analysis goes beyond the scope of our work.

Finally, we assess the impact of antenna settings on the deafness probability. Accordingly, for ULA of isotropic/cosine antenna elements, we apply the Hamming tapering function (also known as a window function), as shown in Fig. 11. The behavior of the resultant curves remains relatively consistent regardless of the variations in the antenna properties, while the deafness probability can be controlled to a certain extent by employing various antenna settings. For instance, the 2x2 array of isotropic elements with the Hamming tapering reduces the deafness probability by up to 45% compared to the Chebyshev tapering. Generally, tapering windows are applied for sidelobe reduction [43] and, hence, for focusing the beam energy more efficiently, which may lead to different large-scale effects depending on the system settings, spatial deployments, and antenna configurations. For example, for "more vertical" 3D links such as those in wearable networks, narrow beams lead to better spatial reuse and increased spectral efficiency. Alternatively, for "more horizontal" connections, the interference in the system may increase, resulting in a deterioration of the system performance. In our formulation, Hamming tapering ensures the smallest peak of the sidelobes, which leads to an increase in the deafness probability. Therefore, the antenna settings that enable a reduction in the deafness probability may, in practice, yield different results for other system parameters, such as spectral efficiency, SINR, etc.

D. *Effects of Radio Settings*

In Fig. 12 and Fig. 13, we study the impact of the antenna pattern on the distance-averaged deafness probability. For example, Fig. 12 illustrates the changes brought by the number of antenna elements for isotropic and cosine antennas and different window functions, such as Hamming, Taylor, and Chebyshev. In general, doubling the antenna size reduces the beamwidth by half and increases the directivity by approximately 3 dB, thus yielding increased deafness probability. As seen in Fig. 12, Chebyshev window function affects the deafness probability differently than Hamming and Taylor functions for both isotropic and cosine antenna elements. Particularly, for 128x128 arrays, the curves corresponding to the Chebyshev tapering decline with a growing number of antenna elements, which can be explained by the specific configuration of the antennas. More precisely, different window functions may result in dissimilar attenuation shapes and coefficients, thus bringing variance in deafness probability values. Here, all curves display a close agreement for smaller numbers of antenna elements, while for larger arrays, Chebyshev tapering results in a lower deafness probability.

In Fig. 13, we explore the impact of the transmit power on the distance-averaged deafness probability for a URA of isotropic antennas. Notably, transmit power P_{tx} affects the selected antenna arrays differently. For example, when P_{tx} increases, the deafness probability is reduced significantly more for the 2x2 array than in other cases. Moreover, the narrower the beams become, the less pronounced the deafness probability decline is. Based on this evaluation, we may conclude that although the dependency of the average deafness probability on the radio-level parameters might seem intuitive, it remains, in fact, susceptible to the selected antenna settings.

This work is licensed under a Creative Commons Attribution 4.0 License. For more information, see https://creativecommons.org/licenses/by/4.0/

This article has been accepted for publication in a future issue of this journal, but has not been fully edited. Content may change prior to final publication. Citation information: DOI 10.1109/TWC.2022.3159086, IEEE Transactions on Wireless Communications

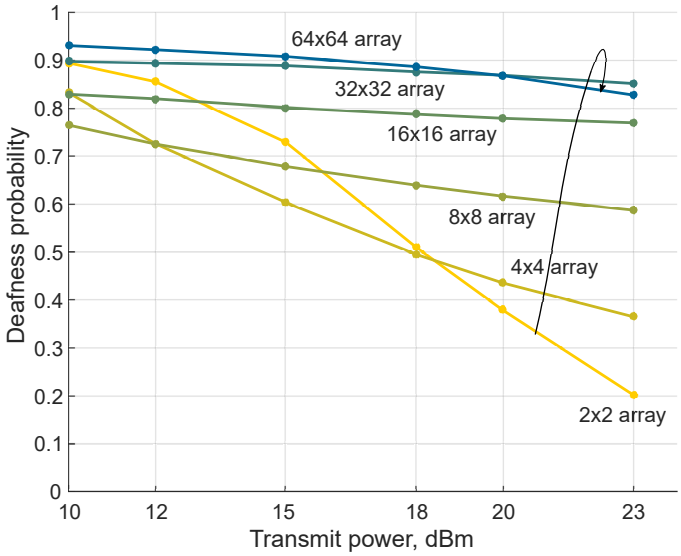

Fig. 13: Impact of transmit power.

VIII. Conclusions

Employing highly directional transmissions in distributed aerial networks (e.g., mmWave-based UAV swarms) significantly increases the chances of directional deafness, which may detrimentally affect the system performance. In this work, we developed a mathematical framework to analyze deafness effects in 3D directional distributed UAV systems. To provide mathematical evaluation for both symmetric and asymmetric drone antenna patterns, we proposed three approximations: (i) a linear model for the antenna pattern and an approximation of the beam coverage by (ii) an ellipse and (iii) an ellipsoid.

Employing stochastic geometry tools, we provided four approaches for evaluating the deafness probability: an integral expression for numerical computation of the distance-dependent deafness probability, its closed-form lower bound, and two expressions for the deafness probability within the ellipse and ellipsoid models. The latter allows considering more complex asymmetric antenna patterns as well as estimating the effects of antenna rotation. We also investigated the impact of the essential system parameters on the 3D directional deafness, which include antenna pattern and shape, number of antenna elements, and tapering functions.

We emphasize that our mathematical methodology remains applicable beyond the considered example scenario. The proposed approximations and their extensions can be utilized for modeling a wide range of UAV-based systems as well as may aid in designing, optimizing, and evaluating radio communications algorithms in emerging aerial 3D deployments. UAV-to-AP association problem is but one example of the proposed methodology extensions. In this case, the output from our framework – estimated deafness probability – can be utilized to evaluate and optimize various association policies. Alternatively, the deafness probability can be used as a criterion to assess the performance of future radio protocol enhancements.

Appendix

In this section, we validate our approximations using simulations based on realistic antenna patterns. In Fig. 14(a), we plot a set of curves illustrating the deafness probability $P_D(d)$ for the following five cases: (i) our analytical model as per (13), (2), (ii) the system-level simulation results, (iii) the linear model as per (5), (iv) the closed-form lower bound as per (14), (15), and (v) the ellipse-based approximation as per (26). The linear model offers a reasonable approximation as it preserves the same trend as the realistic antenna pattern (see "Simulation" curves). The deviation stems from the fact that realistic antenna patterns have more substantial variation due to a higher number of parameters. We emphasize that our lower bound on the deafness probability, which is based on the linear model, agrees well with the simulation results and indeed represents a *lower bound* of the linear approximation as it captures an extended set of antenna patterns.

Further, we evaluate the results of our ellipse-based approach as per (26) under the assumption of symmetric antenna patterns. As noted in Section IV, the antenna pattern varies depending on the beamwidth. In Fig. 14(a), we employ the closest b variations and apply b' from (31) for wider beams (i.e., $\theta > 30°$) and b'' from (32) for narrower beams ($\theta = 8°, 18°$). Even though the difference between the curves in Fig. 14(a) remains noticeable from the quantitative perspective, their essential behavior is similar and repeats the trend for realistic antenna arrays. Therefore, all four approaches, namely, our linear model, numerical analysis, closed-form lower bound, and geometrical ellipse-based approximation, yield adequate results suitable for the UAV systems with centrally symmetric antennas.

In Fig. 14(b), we demonstrate the performance of our ellipsoid-based model as per (34) by controlling the radiation beam pattern in both elevation and azimuth planes for 4x4, 8x8, and 16x16 URAs of isotropic elements (*nearly* axis-symmetric antennas). As one may observe, the results for symmetric and nearly symmetric antennas show a close agreement for the considered system parameters and UAV distributions. We also provide a comparison of the ellipse- and ellipsoid-based approaches, which reveals a perfect match between the results where the antenna pattern has an entirely symmetric form (e.g., for 16x16 array, HPBWs in the horizontal and vertical planes are the same). We highlight that even for nearly symmetric antennas, the absolute deviations from symmetric ones are relatively small, which implies that the developed models accurately capture the deafness probability in the case of URAs.

References

[1] H. Tataria, M. Shafi, A. F. Molisch, M. Dohler, H. Sjöland, and F. Tufvesson, "6G Wireless Systems: Vision, Requirements, Challenges, Insights, and Opportunities," *Proceedings of the IEEE*, 2021.

[2] T. S. Rappaport, Y. Xing, O. Kanhere, S. Ju, A. Madanayake, S. Mandal, A. Alkhateeb, and G. C. Trichopoulos, "Wireless Communications and Applications Above 100 GHz: Opportunities and Challenges for 6G and Beyond," *IEEE Access*, vol. 7, pp. 78729–78757, 2019.

[3] M. Gapeyenko, D. Moltchanov, S. Andreev, and R. W. Heath, "Line-of-Sight Probability for mmWave-based UAV Communications in 3D Urban Grid Deployments," *IEEE Transactions on Wireless Communications*, vol. 20, no. 10, pp. 6566–6579, 2021.

This work is licensed under a Creative Commons Attribution 4.0 License. For more information, see https://creativecommons.org/licenses/by/4.0/

This article has been accepted for publication in a future issue of this journal, but has not been fully edited. Content may change prior to final publication. Citation information: DOI 10.1109/TWC.2022.3159086, IEEE Transactions on Wireless Communications

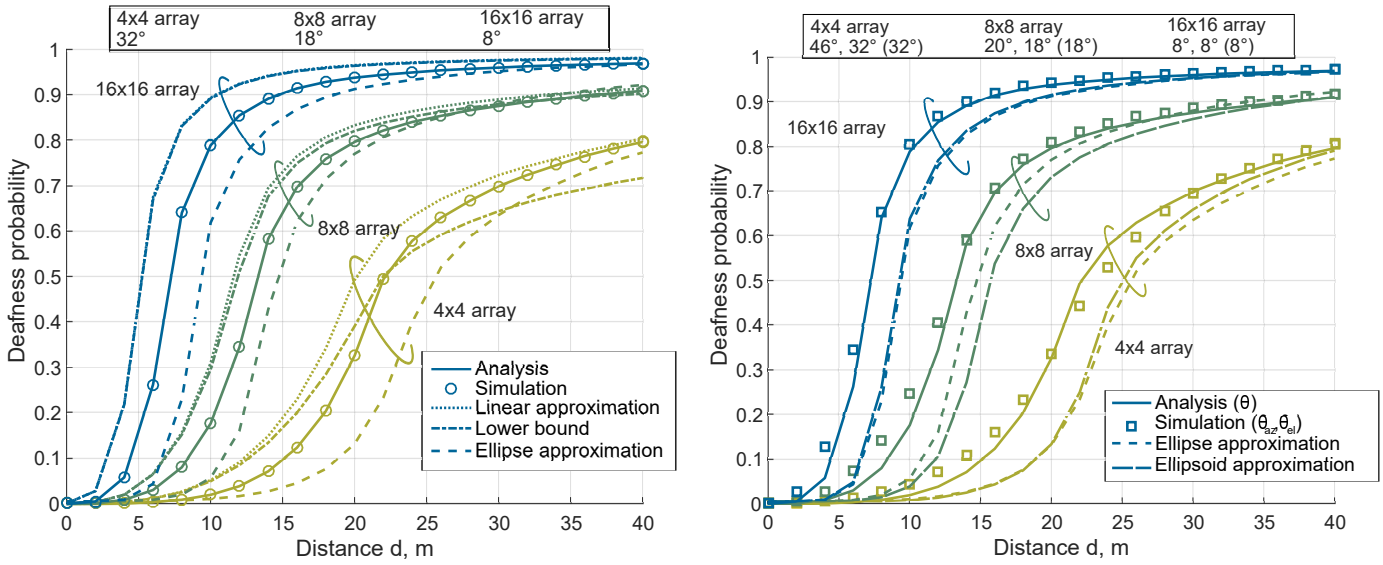

(a) Assessment of approximation solutions for symmetric antenna patterns with URA of isotropic antenna elements.

(b) Comparison of approximation solutions for URA of isotropic antenna elements.

Fig. 14: Deafness probability vs. distance d between A and C.

[4] C. Liu, W. Yuan, Z. Wei, X. Liu, and D. W. K. Ng, "Location-aware Predictive Beamforming for UAV Communications: A Deep Learning Approach," *IEEE Wireless Communications Letters*, vol. 10, no. 3, pp. 668–672, 2020.

[5] J. Hu, C. Chen, L. Cai, M. R. Khosravi, Q. Pei, and S. Wan, "UAV-Assisted Vehicular Edge Computing for the 6G Internet of Vehicles: Architecture, Intelligence, and Challenges," *IEEE Communications Standards Magazine*, vol. 5, no. 2, pp. 12–18, 2021.

[6] "IEEE Standard for Information Technology–Telecommunications and Information Exchange between Systems - Local and Metropolitan Area Networks–Specific Requirements - Part 11: Wireless LAN Medium Access Control (MAC) and Physical Layer (PHY) Specifications," *IEEE Std 802.11-2020 (Revision of IEEE Std 802.11-2016)*, pp. 1–4379, 2021.

[7] Y. Ghasempour, C. R. da Silva, C. Cordeiro, and E. W. Knightly, "IEEE 802.11 ay: Next-Generation 60 GHz Communication for 100 Gb/s Wi-Fi," *IEEE Communications Magazine*, vol. 55, no. 12, pp. 186–192, 2017.

[8] Y. Huo, X. Dong, T. Lu, W. Xu, and M. Yuen, "Distributed and Multi-layer UAV Networks for Next-Generation Wireless Communication and Power Transfer: A Feasibility Study," *IEEE Internet of Things Journal*, vol. 6, no. 4, pp. 7103–7115, 2019.

[9] M. Polese, L. Bertizzolo, L. Bonati, A. Gosain, and T. Melodia, "An Experimental mmWave Channel Model for UAV-to-UAV Communications," in *Proceedings of the 4th ACM Workshop on Millimeter-Wave Networks and Sensing Systems*, pp. 1–6, 2020.

[10] D. B. Johnson and D. A. Maltz, "Dynamic Source Routing in Ad Hoc Wireless Networks," in *Mobile computing*, pp. 153–181, Springer, 1996.

[11] M. Giordani, M. Polese, M. Mezzavilla, S. Rangan, and M. Zorzi, "Toward 6G Networks: Use Cases and Technologies," *IEEE Communications Magazine*, vol. 58, no. 3, pp. 55–61, 2020.

[12] A. Fotouhi, H. Qiang, M. Ding, M. Hassan, L. G. Giordano, A. Garcia-Rodriguez, and J. Yuan, "Survey on UAV Cellular Communications: Practical Aspects, Standardization Advancements, Regulation, and Security Challenges," *IEEE Communications Surveys & Tutorials*, vol. 21, no. 4, pp. 3417–3442, 2019.

[13] L. Zhang, H. Zhao, S. Hou, Z. Zhao, H. Xu, X. Wu, Q. Wu, and R. Zhang, "A Survey on 5G Millimeter Wave Communications for UAV-Assisted Wireless Networks," *IEEE Access*, vol. 7, pp. 117460–117504, 2019.

[14] Q. Zhu, S. Jiang, C.-X. Wang, B. Hua, K. Mao, X. Chen, and W. Zhong, "Effects of Digital Map on the RT-based Channel Model for UAV mmWave Communications," in *2020 International Wireless Communications and Mobile Computing (IWCMC)*, pp. 1648–1653, IEEE, 2020.

[15] W. Xia, V. Semkin, M. Mezzavilla, G. Loianno, and S. Rangan, "Multi-Array Designs for mmWave and Sub-THz Communication to UAVs," in *2020 IEEE 21st International Workshop on Signal Processing Advances in Wireless Communications (SPAWC)*, pp. 1–5, IEEE, 2020.

[16] M. Boschiero, M. Giordani, M. Polese, and M. Zorzi, "Coverage Analysis of UAVs in Millimeter Wave Networks: A Stochastic Geometry Approach," in *2020 International Wireless Communications and Mobile Computing (IWCMC)*, pp. 351–357, IEEE, 2020.

[17] W. Zhong, Y. Gu, Q. Zhu, L. Wang, X. Chen, and K. Mao, "A Novel 3D Beam Training Strategy for mmWave UAV Communications," in *2020 14th European Conference on Antennas and Propagation (EuCAP)*, pp. 1–5, IEEE, 2020.

[18] L. Zhu, J. Zhang, Z. Xiao, X. Cao, X.-G. Xia, and R. Schober, "Millimeter-Wave Full-Duplex UAV Relay: Joint Positioning, Beamforming, and Power Control," *IEEE Journal on Selected Areas in Communications*, vol. 38, no. 9, pp. 2057–2073, 2020.

[19] T. Feng, L. Xie, J. Yao, and J. Xu, "UAV-Enabled Data Collection for Wireless Sensor Networks with Distributed Beamforming," *IEEE Transactions on Wireless Communications*, 2021.

[20] J. Urama, R. Wiren, O. Galinina, J. Kauppi, K. Hiltunen, J. Erkkila, F. Chernogorov, P. Etelaaho, M. Heikkila, J. Torsner, *et al.*, "UAV-Aided Interference Assessment for Private 5G NR Deployments: Challenges and Solutions," *IEEE Communications Magazine*, vol. 58, no. 8, pp. 89–95, 2020.

[21] N. Tafintsev, D. Moltchanov, S. Andreev, S.-p. Yeh, N. Himayat, Y. Koucheryavy, and M. Valkama, "Handling Spontaneous Traffic Variations in 5G+ via Offloading Onto mmWave-Capable UAV "Bridges"," *IEEE Transactions on Vehicular Technology*, vol. 69, no. 9, pp. 10070–10084, 2020.

[22] V. Petrov, M. Gapeyenko, D. Moltchanov, S. Andreev, and R. W. Heath, "Hover or Perch: Comparing Capacity of Airborne and Landed Millimeter-Wave UAV Cells," *IEEE Wireless Communications Letters*, vol. 9, no. 12, pp. 2059–2063, 2020.

[23] Q. Song, Y. Zeng, J. Xu, and S. Jin, "A Survey of Prototype and Experiment for UAV Communications," *Science China Information Sciences*, vol. 64, no. 4, pp. 1–21, 2021.

[24] H. Gossain, C. Cordeiro, D. Cavalcanti, and D. P. Agrawal, "The Deafness Problems and Solutions in Wireless Ad Hoc Networks using Directional Antennas," in *IEEE Global Telecommunications Conference Workshops, 2004. Globecom Workshops 2004.*, pp. 108–113, IEEE, 2004.

[25] X. Wang, L. Kong, F. Kong, F. Qiu, M. Xia, S. Arnon, and G. Chen, "Millimeter Wave Communication: A Comprehensive Survey," *IEEE Communications Surveys & Tutorials*, vol. 20, no. 3, pp. 1616–1653, 2018.

[26] A. P. Subramanian and S. R. Das, "Addressing Deafness and Hidden Terminal Problem in Directional Antenna based Wireless Multi-Hop Networks," *Wireless networks*, vol. 16, no. 6, pp. 1557–1567, 2010.

This work is licensed under a Creative Commons Attribution 4.0 License. For more information, see https://creativecommons.org/licenses/by/4.0/

This article has been accepted for publication in a future issue of this journal, but has not been fully edited. Content may change prior to final publication. Citation information: DOI 10.1109/TWC.2022.3159086, IEEE Transactions on Wireless Communications

[27] G. H. Sim, T. Nitsche, and J. C. Widmer, "Addressing MAC Layer Inefficiency and Deafness of IEEE 802.11ad Millimeter Wave networks Using a Multi-Band Approach," in *2016 IEEE 27th Annual International Symposium on Personal, Indoor, and Mobile Radio Communications (PIMRC)*, pp. 1–6, IEEE, 2016.

[28] Y. Xu, H. Shokri-Ghadikolaei, and C. Fischione, "Distributed Association and Relaying with Fairness in Millimeter Wave Networks," *IEEE Transactions on Wireless Communications*, vol. 15, no. 12, pp. 7955–7970, 2016.

[29] Z. Zheng, A. K. Sangaiah, and T. Wang, "Adaptive Communication Protocols in Flying Ad Hoc Network," *IEEE Communications Magazine*, vol. 56, no. 1, pp. 136–142, 2018.

[30] V. Petrov, G. Fodor, J. Kokkoniemi, D. Moltchanov, J. Lehtomaki, S. Andreev, Y. Koucheryavy, M. Juntti, and M. Valkama, "On Unified Vehicular Communications and Radar Sensing in Millimeter-Wave and Low Terahertz Bands," *IEEE wireless communications*, vol. 26, no. 3, pp. 146–153, 2019.

[31] O. Galinina, A. Pyattaev, K. Johnsson, S. Andreev, and Y. Koucheryavy, "Analyzing Effects of Directional Deafness on mmWave Channel Access in Unlicensed Bands," in *2017 IEEE Globecom Workshops (GC Wkshps)*, pp. 1–7, IEEE, 2017.

[32] O. Chukhno, N. Chukhno, O. Galinina, Y. Gaidamaka, S. Andreev, and K. Samouylov, "Analysis of 3D Deafness Effects in Highly Directional mmWave Communications," in *2019 IEEE Global Communications Conference (GLOBECOM)*, pp. 1–6, IEEE, 2019.

[33] T. Cai, J. Fan, and T. Jiang, "Distribution of Angles in Random Packing on Spheres," in *2013 J. Mach. Learn. Res. 14*, pp. 1837–1864, 2013.

[34] A. Alkhateeb, G. Leus, and R. W. Heath, "Compressed sensing based multi-user millimeter wave systems: How many measurements are needed?," in *2015 IEEE international conference on acoustics, speech and signal processing (ICASSP)*, pp. 2909–2913, IEEE, 2015.

[35] N. Deng and M. Haenggi, "A Novel Approximate Antenna Pattern for Directional Antenna Arrays," *IEEE Wireless Communications Letters*, vol. 7, no. 5, pp. 832–835, 2018.

[36] H. Wei and N. Deng, "A Simple yet Effective Approximation for Directional Antenna Arrays," in *2018 24th Asia-Pacific Conference on Communications (APCC)*, pp. 476–481, IEEE, 2018.

[37] J. D. Krauss and R. J. Marhefka, "Antennas for All Applications," *McGraw-Hill*, pp. 378–379, 2002.

[38] IEEE 802.11 Working Group, "Wireless LAN Medium Access Control (MAC) and Physical Layer (PHY) Specifications. Amendment 3: Enhancements for Very High Throughput in the 60 GHz Band," 2012.

[39] IEEE 802.11 Working Group, "Enhanced Throughput for Operation in License-exempt Bands Above 45 GHz," tech. rep., IEEE P802.11ay/D0.3, Mar. 2017.

[40] "IEEE Draft Standard for Information Technology-Telecommunications and Information Exchange Between Systems - Local and Metropolitan Area Networks-Specific Requirements Part 11: Wireless LAN Medium Access Control (MAC) and Physical Layer (PHY) Specifications-Amendment 2: Enhanced Throughput for Operation in License-Exempt Bands Above 45 GHz," *IEEE P802.11ay/D7.0*, pp. 1–784, Dec. 2020.

[41] H. Assasa and J. Widmer, "Extending the IEEE 802.11 ad Model: Scheduled Access, Spatial Reuse, Clustering, and Relaying," in *Proceedings of the Workshop on Ns-3*, pp. 39–46, 2017.

[42] S. Niknam and B. Natarajan, "On the Regimes in Millimeter Wave Networks: Noise-Limited or Interference-Limited?," in *2018 IEEE International Conference on Communications Workshops (ICC Workshops)*, pp. 1–6, IEEE, 2018.

[43] R. Haupt, "Reducing Grating Lobes Due to Subarray Amplitude Tapering," *IEEE Transactions on Antennas and Propagation*, vol. 33, no. 8, pp. 846–850, 1985.

Olga Chukhno is an Early Stage Researcher within H2020 MCSA ITN/EJD A-WEAR project and a PhD student at Mediterranea University of Reggio Calabria, Italy and Tampere University, Finland. She received M.Sc. (2019) in Fundamental Informatics and Information Technologies and B.Sc. (2017) in Business Informatics from RUDN University, Russia. Her current research interests include wireless communications, social networking, edge computing, and wearable applications.

Nadezhda Chukhno is an Early Stage Researcher at A-WEAR and Doctoral Researcher at Mediterranea University of Reggio Calabria, Italy and Jaume I University, Spain. She graduated from RUDN University, Russia, and received her B.Sc. in Business Informatics (2017) and M.Sc. in Fundamental Informatics and Information technologies (2019). Her current research activity mainly focuses on wireless communications, 5G+ networks, multicasting, D2D, and wearable technologies.

Olga Galinina is a Senior Research Fellow at Tampere University. She received her B.Sc. and M.Sc. degrees from the Department of Applied Mathematics, St. Petersburg State Polytechnical University of Peter the First, Russia and the Ph.D. degree from Tampere University of Technology (TUT) in 2015. Her research interests include applied mathematical modeling and analysis of wireless networks and statistical machine learning.

Sergey Andreev is an associate professor of communications engineering and Academy Research Fellow at Tampere University, Finland. He received his Ph.D. (2012) from TUT as well as his Specialist (2006), Cand.Sc. (2009), and Dr.Habil. (2019) degrees from SUAI. He has been a Visiting Senior Research Fellow with King's College London, UK (2018-20) and a Visiting Postdoc with University of California, Los Angeles, US (2016-17). He (co-)authored more than 200 published research works on intelligent IoT, mobile communications, and heterogeneous networking.

Yuliya Gaidamaka received a PhD in 2001 and a Full Doctor of Sciences degree in 2017 in Mathematics from the Peoples' Friendship University of Russia (RUDN University). Since 2001, she has been an associate professor and currently a professor in the university's Applied Probability and Informatics Department. She is the author of more than 200 scientific and conference papers, co-author of three monographs on multiplicative solutions of finite Markov chains, matrix and analytical methods for performance analysis of wireless heterogeneous networks. Her current research focuses on performance analysis of 5G+ networks, queuing theory, mathematical modeling of communication networks including admission control, radio resource management using artificial intelligence.

Konstantin Samouylov received his Ph.D. degree from the Moscow State University and Doctor of Sciences degree from the Moscow Technical University of Communications and Informatics. During 1985–1996, he held several positions at the Faculty of Sciences of the Peoples' Friendship University of Russia where he became the head of the Telecommunication Systems Department in 1996. From 2014, he became the head of the Department of Applied Informatics and Probability Theory of RUDN University (previously named PFUR). During last two decades, Konstantin Samouylov has been conducting research projects for the Helsinki and Lappeenranta Universities of Technology, Moscow Central Science Research Telecommunication Institute, several Institutes of Russian Academy of Sciences and a number of Russian network operators. His current research interests are performance analysis of 4G networks (LTE, WiMAX), teletraffic of triple play networks, signalling network (SIP) planning, and cloud computing. He has written more than 150 scientific and technical papers and three books.

Giuseppe Araniti (Senior Member, IEEE) received the Laurea degree and the Ph.D. degree in electronic engineering from the University Mediterranea of Reggio Calabria, Italy, in 2000 and 2004, respectively. He is currently an Associate Professor of telecommunications with the University Mediterranea of Reggio Calabria. His major area of research is on 5G/6G networks and it includes personal communications, enhanced wireless and satellite systems, traffic and radio resource management, multicast and broadcast services, device-to-device (D2D), and machine-type communications (M2M/MTC).

This work is licensed under a Creative Commons Attribution 4.0 License. For more information, see https://creativecommons.org/licenses/by/4.0/